Theoretical study of the low-lying electronic states of CCCF radical and its ions

RESEARCH · JUNE 2015

DOI: 10.13140/RG.2.1.3429.6481

Computational and Theoretical Chemistry 964 (2011) 277–282

Contents lists available at ScienceDirect

Computational and Theoretical Chemistry

journal homepage: www.elsevier.com/locate/comptc

Theoretical study of the low-lying electronic states of CCCF radical and its ions

Ming-Xing Song, Zeng-Xia Zhao, Wei Zhang, Fu-Quan Bai, Hong-Xing Zhang *, Chia-Chung Sun

Institute of Theoretical Chemistry, State Key Laboratory of Theoretical and Computational Chemistry, Jilin University, Changchun 130023, PR China

ARTICLE INFO

Article history:
Received 3 November 2010
Received in revised form 17 December 2010
Accepted 6 January 2011
Available online 12 January 2011

Keywords:
CCCF
CASSCF
Excited state
Radidal

ABSTRACT

The low-lying electronic states of the CCCF radical and its ionic states have been investigated systematically using the complete active space self-consistent field (CASSCF) and multiconfiguration second-order perturbation theory (CASPT2) methods in conjunction with aug-cc-pVTZ basis set. To investigated the Renner–Teller effect on the CCCF radical, C_s symmetry was used for CCCF. The CCCF has been found to have a X^2A' ground state with rotational constant $\overline{B}$ = 4500.5 MHz, which is in good agreement with the experimental values of 4555.8043 MHz. The calculations of vertical excitation energies of CCCF at 2.893 and 4.180 eV are attribute to the $X^2A' \rightarrow 3^2A''$ and $X^2A' \rightarrow 5^2A'$, respectively, which has larger oscillator strengths. The ionization potentials of CCCF are computed in order to provide a theoretical guidance to the photoelectron spectrum (PES) of the CCCF radical. The first adiabatic electron affinity (AEA) of CCCF is predicted to be 2.671 eV. A comparison of the geometries and bonding among the CCCX (X = F, Cl, and Br) radicals presents the ground state X^2A' of CCCX can be described as allenic structures with the unpaired electron on the C3 atom, while the excited state $1^2A''$ ($1^2\Pi$) of CCCX have the linear acetylenic structures with the unpaired electron on the C1 atom. The barriers to linearity decrease as follows: ΔE (CCCF) < ΔE (CCCCl) < ΔE (CCCBr).

1. Introduction

In the past two decades, the heteroatom-doped carbon-chain radicals have been widely investigated spectroscopically due to their potential astrophysical interest [1–10]. Indeed, many of such radicals have been detected in various interstellar media, for example, C_3H[3], C_3N[4], C_3O[5], and C_3S[6] have been detected in TMC-1 and IRC+10216. For this reason, more and more experimental and theoretical studies have been focused on these species. Among the carbon-chain bearing halogen atoms, the C_nCl have been received extensive attention [11–26]; possibly due to the fact the Cl is a relatively abundant element. The CCCCl have been studied by electronic absorption spectroscopy trapped in Ne matrices [21,22], and Fourier-transform microwave spectroscopy [23]. Several theoretical studies on the equilibrium geometry and excited energies have been reported [23–26].

Similarly, a joint experimental/theoretical study produced pure rotational transitions of another carbon-chain radical bearing halogen atom, CCCF, using a Fourier-transform microwave spectrometer with a pulsed-discharge nozzle [27]. The study showed that the bent ground state, X^2A', and the linear first excited state, $1^2A''$ ($1^2\Pi$), form a Renner–Teller pair, degenerate in the linear geometry. To the best of our knowledge there are no experimental or theoretical studies on its ionic states. In this paper, we give a high-level *ab initio* calculations about the properties of CCCF radical, except for the structure, transition strength and vibrational frequencies of neutral, cationic, and anionic species, respectively; we also calculated the ionization energies about CCCF radical. All the calculations at the CASSCF/CASPT2 level of theory, which have been shown to provide accurate interpretation and predication for the excited states in numerous applications in our previous work [28–36], and the results show good agreement with the available observed values.

2. Methodology

The geometries of the low-lying electronic states of CCCF radical, $CCCF^+$ cation, and $CCCF^-$ anion have been investigated via complete active space self-consistent field (CASSCF) [37] method. Second-order perturbation (CASPT2) [38] calculations were performed to consider the dynamic correction, which takes the CASSCF wave functions as a reference in the second-order perturbation treatment. The multiconfigurational linear response (MCLR) [39] was used to calculate the harmonic vibrational frequencies.

The augmented correlation consistent basis set aug-cc-pVTZ basis set developed by Dunning and co-workers was used in the calculation [40]. The aug-cc-pVTZ basis set consists of 184 contracted basis functions with a contracted scheme of C, F (11s6p3d2f/5s4p3d2f).

Consider the Renner–Teller effect in CCCF radical, all calculations were carried out in C_s symmetry. The selection of the active space is a crucial step in a CASSCF/CASPT2 calculation. In probe SCF, calculation of the electronic configuration of the neutral ground radical is

* Corresponding author.
E-mail address: zhanghx@mail.jlu.edu.cn (H.-X. Zhang).

2210-271X/$ - see front matter © 2011 Elsevier B.V. All rights reserved.
doi:10.1016/j.comptc.2011.01.005

confirmed as [core](5a′)^2(6a′)^2(7a′)^2(8a′)^2(9a′)^2(1a″)^2(10a′)^2(11a′)^2(2a″)^2(12a′)$^\alpha$, in which [core] denotes as (1a′)^2(2a′)^2(3a′)^2(4a′)^2. To keep a balance between the computation cost and the computation precise, the active spaces including 13 electrons in 13 orbitals is selected in the construction of CASSCF wavefunctions, which means nine a′ orbitals and four a″ orbitals. The same active space was chosen for the C_3F^+ and C_3F^-.

The CAS state interaction (CASSI) [41] method was employed to compute the transition dipole moments, which were combined with CASPT2 energy differences to obtain oscillator strengths.

The optimized geometry of the ground state of C_3F was used to calculate the vertical ionization energies, which are obtained from the difference of the total energies between the resulting radical cations and the neutral C_3F radical. The calculated electron affinities are obtained from the difference of the total energies between the neutral C_3F radicals and the radical anion in their respective optimized geometries. All of the calculations were performed using the MOLCAS 6.0 suite of programs [42].

3. Results and discussion

3.1. CCCF

3.1.1. Geometries

To determine the Renner–Teller effect, we have calculated the states with a C_s symmetry constraint. In Table 1 we exhibit the optimized geometries, configuration, energy separations and dipole moment for the ground state and low-lying electronic excited states of CCCF in C_s symmetry at the CASSCF/CASPT2 level. And in Table 2, we listed the Mulliken spin population analysis for X^{2}A′, 1^{2}Π (1^{2}A″), 1^{4}A′ and 1^{4}A″ of CCCF.

The lowest 1^{2}Π state of CCCF is found to have a C1—C2 bond length of 1.364 Å, a C2—C3 bond distance of 1.228 Å, and C3—F bond length of 1.272 Å within our CASSCF approach. The dipole moment of the 1^{2}Π state is 2.9 D. These can be compared to theoretical values of Takashi et al. [27]. The 1^{2}Π state presents one real (514.5 cm^{-1}) and one imaginary vibrational frequency (200.3i cm^{-1}) along the CCF bending coordinates, and the eigenvector of the imaginary vibrational frequency leads to a trans-planar bent structure for the lowest electronic state X^{2}A′. The component of the 1^{2}Π state with the real bending vibrational frequency is assigned to the 1^{2}A″ (1^{2}Π) state. That is, the 1^{2}Π state undergoes a Renner–Teller splitting to display two electronic states, the first Renner–Teller component X^{2}A′ experiences a strong stabilization upon reducing the ∠C2C3F from 180.0° to the equilibrium values of 134.9°, leading a barrier of 0.385 eV (3106 cm^{-1}), which can be compared with the value of 3200 cm^{-1}. Therefore, the 1^{2}Π state of CCCF is a type of C Renner–Teller molecule as proposed by Lee et al. [43]. The rotational constant ($\bar{B}$) of X^{2}A′ state for CCCF radical is predicted to be 4500.5 MHz, which is accordance with the available experimental value of 4555.8043 MHz, indicating that the CASSCF/CASPT2(13,13)/aug-cc-pVTZ level is reliable. The ground state X^{2}A′ has a mainly electronic configuration (core)(5a′)^2(6a′)^2(7a′)^2(8a′)^2(1a″)^2(9a′)^2(10a′)^2(11a′)^2(2a″)^2(12a′)$^\alpha$ with a coefficient of 0.91. As shown in Table 2, our calculations gave C1 and C3 atom spin densities of 0.3543 and 0.7810 for the ground state X^{2}A′ state for CCCF, respectively. The two short C—C bond distances suggests double-bond character, therefore, the electronic structure can be describe as C=C=Ċ—F.

Due to a single excitation 12a′ MO (π^*(π(C1—C2)—C3—F)) to 3a″ MO (π^*(π(C1—C2)—C3—F)), the R_{C1C2} bond length for the 1^{2}A″ (1^{2}Π) is longer than that for X^{2}A′ state, and R_{C2C3} and R_{C3F} is shorten by 0.083 and 0.024 Å, respectively. The first excited state of CCCF presents the ∠C2C3F bond angle of 180.0°. The dipole moment of the X^{2}A′ and 1^{2}A″ (1^{2}Π) states are calculated to be 2.6 and 3.1 D, respectively. It can be seen that the CCCF radical is the most polar at the linear configuration and the deviation from the linearity significantly decrease the magnitude of the dipole moment. Our calculations gave C1 and C3 atom spin densities of 0.7618 and 0.3846 for the ground state X^{2}A′ state for CCCF, respectively. The short R_{C2C3} (1.225 Å) indicates a triple bond character, which can be described as ·C—C≡C—F.

Table 2
Mulliken spin population analysis for X^{2}A′, 1^{2}Π (1^{2}A″), 1^{4}A′ and 1^{4}A″ of CCCF.

Atom	Orbital	State			
		X^{2}A′	1^{2}Π (1^{2}A″)	1^{4}A′	1^{4}A″
C1	1s	−0.0006	0.0152	−0.0025	0.4128
	2px	0.3543	0.0046	0.0937	0.4586
	2py	0.0186	−0.0055	−0.0082	0.5433
	2pz	−0.0194	0.7533	0.5208	0.6020
	Total	0.3543	0.7618	0.6286	2.0147
C2	1s	−0.0007	−0.0023	0.0248	0.0274
	2px	−0.0811	−0.0184	−0.0475	−0.2309
	2py	−0.0182	−0.0083	−0.0162	−0.0444
	2pz	−0.0445	−0.1076	0.5120	−0.2463
	Total	−0.1640	−0.1634	0.4770	−0.5358
C3	1s	0.2217	0.0074	0.3492	0.2770
	2px	0.3491	0.0159	0.3785	0.4199
	2py	0.1297	0.0081	0.1745	0.1287
	2pz	0.0712	0.3573	0.8593	0.6357
	Total	0.7810	0.3846	1.7948	1.4732
F	1s	0.0009	−0.0025	0.0029	−0.0004
	2px	0.0229	−0.0019	0.0351	0.0128
	2py	−0.0007	−0.0094	0.0002	−0.0069
	2pz	0.0006	0.0291	0.0515	0.0337
	Total	0.0287	0.0170	0.0996	0.0479

Table 1
Geometries parameters (bond distance in Å and bond angle in °), leading configurations (the weights exceed 5%), the CI coefficients, adiabatic excitation energies (T_a) (in eV) and dipole moment (in D) for low-lying electronic states of CCCF using CASSCF/CASPT2 methods with aug-cc-pVTZ basis set.

State	R_{C1C2}	R_{C2C3}	R_{C3F}	∠C1C2C3	∠C2C3F	Configuration[a]		T_a CASSCF	T_a CASPT2	Dipole moment
						Occupied	Coef.			
X^{2}A′	1.296	1.308	1.292	163.3	134.9	(10a′)^2(2a″)^2(11a′)^2(12a′)$^\alpha$(3a″)^0	0.91			2.6
RCCSD(T)/cc-pVQZ[b]	1.297	1.301	1.284	163.5	134.8					2.5
1^{2}Π	1.364	1.228	1.272	180.0	180.0	(2π)^4(9σ)^2(3π)$^\alpha$	0.94	1.135	0.385 (3106 cm^{-1})	2.9
RCCSD(T)/cc-pVQZ[b]	1.348	1.237	1.265	180.0	180.0				3200 cm^{-1}	3.2
1^{2}A″ (1^{2}Π)	1.347	1.225	1.268	180.0	180.0	(10a′)^2(2a″)^2(11a′)^2(12a′)^0(3a″)$^\alpha$	0.93	0.407	0.607	3.1
1^{4}A″	1.265	1.321	1.317	165.0	132.5	(10a′)^2(2a″)^2(11a′)$^\alpha$(12a′)$^\alpha$(3a″)$^\alpha$	0.93	1.407	1.501	1.0
1^{4}A′	1.296	1.424	1.316	173.5	124.4	(10a′)^2(2a″)$^\alpha$(11a′)^2(12a′)$^\alpha$(3a″)$^\alpha$	−0.96	2.173	3.213	2.6

[a] In active orbitals 'α' represents a singly occupied orbital containing an electron with an up spin, 'β' represents a singly occupied orbital containing an electron with a down spin. The common configuration (core)(6σ)^2(7σ)^2(8σ)2(1π)^2 is not presented for the linear states, and [core](5a′)^2(6a′)^2(7a′)^2(8a′)^2(9a′)^2(1a″)^2 is not presented for the tans-planar bent states.
[b] Taken from Ref. [27].

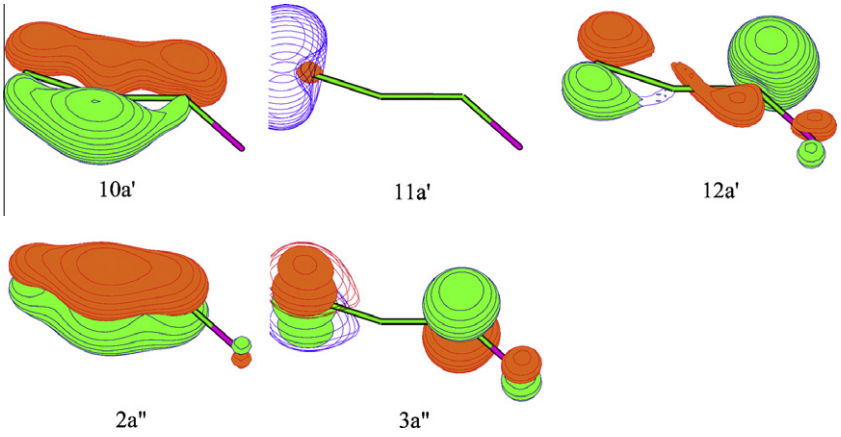

Fig. 1. The plots of densities for a part of CCCF orbitals included in the active space.

For the quartet CCCF radical, we locate two trans-planar bent electronic states. As can be seen from Table 1 and Fig. 1, one electron in the 11a′ MO (*n*(C: 2spxpy)) is promoted to the 3a″ resulting in the formation of $1^4A''$ quartet state. Consequently, the R_{C1C2} is shortened by 0.031 Å, the R_{C2C3} and R_{C3F} are lengthened by 0.013 and 0.025 Å, respectively. Owing the 2a″ → 3a″ single excitation, the R_{C2C3} and R_{C3F} bond lengths of $1^4A'$ are longer than those of X^2A'. The bond distance, bond angles and spin densities (Table 2) suggest that the $1^4A''$ state of CCCF basically consist of a $\dot{C}$═C conterpart and $\dot{C}$—F radical, who can be describe as $\dot{C}$═C—$\dot{C}$—F, while the electronic structure of $1^4A'$ state can be qualitatively descried as C═C—$\dot{C}$—F.

There are no cis CCCF doublets or quartet structures were located.

3.1.2. Harmonic vibrational frequencies

The harmonic vibration frequencies of calculated states of CCCF were listed in Table 3. There are six frequencies involved, three types of stretching vibrations (ω_1, ω_2, and ω_3), and three types of bending vibrations (ω_4 (CCF bending), ω_5 (a′) (CCC in-plane bending), and ω_5 (a″) (out-of-plane CCC bending)). The CCF bending frequency (ω_4 = 532.7 cm^{-1}) is largest in calculated electronic states due to the smallest CCF bond angle of the $1^4A'$ state (∠C2C3F = 124.4°). Except for the $1^2A''$ ($1^2\Pi$) state, all the calculated electronic states are true minimum on the PES.

3.1.3. Vertical excitation energies

According to the Franck–Condon principle, the vertical transition energies (T_v) and corresponding oscillator strengths (*f*) of eleven doublet and six quartet excited states of CCCF radical were calculated by the SA-CASSCF/CASPT2 method with aug-cc-pVTZ basis set, together with the previous calculations, are summarized in Table 4. Among the eleven doublet excitation states considered here, the lowest one is found to be $1^2A''$, and $X^2A' \rightarrow 1^2A''$ transition is predicted at 1.225 eV (9880 cm^{-1}) with $f = 5.22 \times 10^{-4}$, very close to the calculated value (10,000 cm^{-1}) [27]. The more intensive transition of $X^2A' \rightarrow 3^2A''$ and $X^2A' \rightarrow 5^2A'$ occurs at 2.893 and 4.180 eV with $f = 5.98 \times 10^{-3}$ and 9.97×10^{-3}, respectively. The results show that the $1^4A''$, $1^2A''$, $2^2A'$, $3^2A''$, $1^4A'$, $4^2A''$, $5^2A''$, and $4^2A'$ excited states mainly caused by single configuration transition, the others excited states present obviously multiconfigurational character. Unfortunately, there are no experimental values for comparing.

Table 3
Harmonic frequencies for the ground and excited states of CCCF calculated by MCLR.

State	ω_1	ω_2	ω_3	ω_4 (CCF bending)	ω_5 (CCC bending)	
					a′	a″
X^2A'	1923.3	1450.6	952.3	520.7	211.9	145.2
$1^2\Pi$	2176.7	1361.3	824.3	514.5/200.3i	292.4	211.0
$1^2A''$ ($1^2\Pi$)	2179.2	1400.5	848.2	379.4/379.8i	179.9	283.1
$1^4A''$	1656.9	1448.4	906.7	527.7	226.2	338.4
$1^4A'$	1824.1	1350.7	915.8	532.7	176.8	229.4

3.2. $CCCF^+$ and $CCCF^-$

3.2.1. Geometries

Because $CCCF^+$ is the product from the photoelectron ionization of the CCCF, the ground and excited states of $CCCF^+$ using the same basis sets and methods as the neutral molecules were calculated. On the basis of adiabatic energies, the X^1A' ($1^1\Sigma^+$) is confirmed as the ground state of $CCCF^+$, which is predicted to be linear in this

Table 4
Vertical excitation energies T_v (eV) and oscillator (*f*) for CCCF by CASSCF/CASPT2/aug-cc-pVTZ.

State	Transition	T_v	*f*
X^2A'		0.000	
12A″	12a′ → 3a″	1.225 (9880 cm^{-1}) (10,000 cm^{-1})[a]	5.22×10^{-4}
$1^4A''$	11a′ → 3a″	1.333	$<10^{-10}$
$2^2A'$	11a′ → 12a′	2.096	1.92×10^{-3}
$2^2A''$	12a′ → 3a″ (10a′)(11a′) → (12a′)(3a″)	2.357	1.76×10^{-3}
$3^2A''$	11a′ → 3a″	2.893	5.98×10^{-3}
$1^4A'$	2a″ → 3a″	2.909	$<10^{-10}$
$3^2A'$	11a′ → 12a′ 2a″ → 3a″	2.851	1.23×10^{-3}
$2^4A''$	11a′ → 3a″ 10a′ → 3a″	2.953	$<10^{-10}$
$4^2A''$	2a″ → 12a′	3.450	6.39×10^{-4}
$5^2A'$	11a′ → 12a′ 2a″ → 3a″	4.180	9.97×10^{-3}
$5^2A''$	11a′ → 3a″	3.714	3.61×10^{-4}
$4^2A'$	2a″ → 3a″	3.957	1.58×10^{-3}
$3^4A''$	(10a′)(11a′) → (12a′)(3a″) 11a′ → 14a′	4.661	$<10^{-10}$
$6^2A'$	$(11a')(12a') \rightarrow (3a'')^2$	4.613	2.98×10^{-4}
$2^4A'$	(11a′)(2a″) → (12a′)(3a″)	4.725	
$6^2A''$	11a′ → 3a″ $(11a')(2a'') \rightarrow (3a'')^2$	5.065	1.44×10^{-4}
	(11a′)(2a″) → (12a′)(3a″)	5.295	$<10^{-10}$
$3^4A'$	11a′ → 13a′ 10a′ → 13a′		

[a] Taken from Ref [27].

work. Compared with the ground state of neutral radical, this state can result from eliminating the single electron in the 12a′ orbital of the CCCF, which elongates the R_{C1C2} bond distance, and shortens the R_{C2C3} and R_{C3F} bond lengths.

It can be seen from Table 5 that the absolute values of configuration coefficient for the $1^3A'$, $1^3A''$, and $1^1A''$ states are above 0.91, indicating a single-reference character of the respective states. The single excitation from the nonbonding MO (11a′) to antibonding MO (12a′) shortens the R_{C1C2} distance and lengths the R_{C2C3} bond distance for the $1^3A'$ state. The electron promoted from 2a″ MO to the 12a′ in parallel and unparallel produce the $1^3A''$ and $1^1A''$ states, respectively. Therefore, structures $1^3A''$ and $1^1A''$ states have significantly longer R_{C1C2} and R_{C2C3} bond distances than that of X^1A' ($1^1\Sigma^+$) state.

Structures of X^1A' ($1^1\Sigma^+$), $1^3A'$, and $1^1A''$ states are true equilibrium geometries, since there are no imaginary frequencies as shown in Table 6. The $1^3A''$ state presents an imaginary vibrational frequency for the CCC bending mode (ω_5 = 239.8i). Consequently, it denotes a first-order saddle point on the PES.

The X^1A' ground state of $CCCF^-$ is strongly bent (∠C1C2C3=169.1°, and ∠C2C3F = 110.4°) and exhibits an adiabatic electron affinity (AEA) of 2.671 eV. The X^1A' ground state of $CCCF^-$ has a dominant leading configuration (core)$(6a')^2(7a')^2(8a')^2(9a')^2(1a'')^2(10a')^2(2a'')^2(11a')^2(12a')^2(3a'')^0$ with a coefficient of 0.94. As compared to the ground state X^2A' of CCCF neutral radical, this state is mainly created by adding a single electron to the antibonding 12a′ orbital. The addition of electron increased the interaction of the 12a′ MO, which makes the R_{C1C2} shortened and R_{C2C3} and R_{C3F} elongated in the $CCCF^-$ anion. The CCF bending frequency is larger for the X^1A' state (616.7 cm^{-1}, shown in Table 6) of $CCCF^-$ than the X^2A' of CCCF (520.7 cm^{-1}) due to the smaller CCF bond angle of the X^1A' state for the $CCCF^-$.

As shown in Table 5, the absolute value of coefficient for the $1^3A''$, $1^1A''$, and $1^3A'$ of the $CCCF^-$ leading configurations are above 0.92, indicating a single configuration character of the respective states. The $2^1A'$ state show obvious multiconfiguration character. Compared with the leading configuration of the ground state X^1A' of $CCCF^-$, the $1^3A''$ and $1^1A''$ states can be regarded as the results of the single electron excitation 12a′ → 3a″, therefore, the two states have similar structures. The R_{C1C2} and R_{C3F} bond lengths of $1^3A''$ and $1^1A''$ states are longer than those of X^1A' state, and the R_{C2C3} bond length of $1^3A''$ and $1^1A''$ states is shorten than that of X^1A' state. Owing to the $(12a')^2 \rightarrow (3a'')^2$ double electron excitations in Table 5, the R_{C1C2} bond distance of $2^1A'$ state increases, while the R_{C2C3} and R_{C3F} bond lengths decrease. Due to as single excitation from 2a″ MO to 3a″ MO, the bonding interaction of C2, C3 and F atoms of $1^3A'$ state are badly impaired, and R_{C2C3} and R_{C3F} are strongly longer than that of X^1A' state. The CASSCF/CASPT2 T_a values of $1^1A''$ and $2^1A'$ are predicted at 1.689 and 2.833 eV. The magnitude of the dipole moment for anion is larger than the ground state X^2A' of CCCF. All the calculated anionic states have no imaginary, indicating true minimum points on the PES.

Table 6
Harmonic frequencies for the ground and excited states of $CCCF^+$ and $CCCF^-$ calculated by MCLR.

State	ω_1	ω_2	ω_3	ω_4 (CCF bending)	ω_5 (CCC bending)	
					a′	a″
$CCCF^+$						
$X^1A'(1^1\Sigma^+)$	2383.0	1703.6	910.8	471.4	161.4	
$1^3A'$	2041.6	1665.1	1002.7	530.7	233.4	212.9
$1^3A''$	1699.1	1578.8	978.3	544.7	203.5	239.8i
$1^1A''$	1696.7	1532.7	963.8	538.8	232.6	210.7
$CCCF^-$						
X^1A'	1908.5	1113.8	1009.1	616.7	216.2	215.2
$1^3A''$	1648.8	1262.1	887.3	542.5	221.1	365.9
$1^1A''$	1705.3	1256.0	861.0	553.7	221.8	257.0
$2^1A'$	1982.1	1276.3	780.0	508.7	242.8	324.1
$1^3A'$	1634.8	904.1	824.3	564.4	215.5	512.2

Table 7
The calculated vertical and adiabatic IPs of CCCF.

State	AIPs	VIPs
X^1A'	9.452	10.362
$1^3A'$	10.864	11.013
$2^1A'$		11.560
$2^3A'$		12.419
$1^3A''$	12.376	12.608
$2^3A''$		12.629
$1^1A''$	12.638	12.943
$2^1A''$		13.126
$3^1A'$		13.482
$3^3A'$		13.836
$3^3A''$		14.135
$3^1A''$		14.408

3.2.2. Ionization potential

There are no experimental and calculated data available for the information of the $CCCF^+$ cation. The first ionization potential of CCCF corresponds to the X^1A' state of the $CCCF^+$ cation. Comparing with the configurations of ground state of the CCCF shown in Table 1 with those of the cation shown in Table 5, we can see that this ionization is mainly generated by removing the 12a′ electron from the dominant leading configuration of CCCF. The calculated adiabatic ionization energies and vertical energies were summarized in Table 7. The calculated first/second adiabatic and vertical IPs is 9.452/10.864 eV and 10.362/11.013 eV, respectively.

Table 5
Geometries parameters (bond distance in Å and bond angle in °), leading configurations (the weights exceed 5%), the CI coefficients, adiabatic excitation energies (T_a) (in eV) and dipole moment (in D) for low-lying electronic states of $CCCF^+$ and $CCCF^-$ using CASSCF/CASPT2 methods with aug-cc-pVTZ basis set.

State	R_{C1C2}	R_{C2C3}	R_{C3F}	∠C1C2C3	∠C2C3F	Configuration		T_a (CASSCF)	T_a (CASPT2)	Dipole moment
						Occupation	Coef.			
$CCCF^+$										
$X^1A'(1^1\Sigma^+)$	1.314	1.227	1.220	180.0	180.0	$(2\pi)^4(9\sigma)^2(3\pi)^0$	0.93			3.3
$1^3A'$	1.236	1.339	1.229	157.5	134.5	$(10a')^2(2a'')^2(11a')^{\alpha}(12a')^{\alpha}(3a'')^0$	−0.90	1.344	1.412	4.2
$1^3A''$	1.338	1.377	1.226	159.0	131.3	$(10a')^2(2a'')^{\alpha}(11a')^2(12a')^{\alpha}(3a'')^0$	−0.92	2.756	2.925	1.8
$1^1A''$	1.344	1.384	1.222	154.5	131.5	$(10a')^2(2a'')^{\beta}(11a')^2(12a')^{\alpha}(3a'')^0$	−0.91	2.969	3.186	1.5
$CCCF^-$										
X^1A'	1.281	1.395	1.353	169.1	110.4	$(10a')^2(2a'')^2(11a')^2(12a')^2(3a'')^0$	0.94			5.8
$1^3A''$	1.297	1.351	1.371	169.9	129.8	$(10a')^2(2a'')^2(11a')^2(12a')^{\alpha}(3a'')^{\alpha}$	0.92	0.607	0.825	8.9
$1^1A''$	1.328	1.317	1.372	172.0	131.7	$(10a')^2(2a'')^2(11a')^2(12a')^{\alpha}(3a'')^{\beta}$	0.93	1.740	1.689	8.2
$2^1A'$	1.359	1.259	1.339	175.7	159.6	$(10a')^2(2a'')^2(11a')^2(12a')^2(3a'')^0$	0.42	3.224	2.833	9.5
						$(10a')^2(2a'')^2(11a')^2(12a')^0(3a'')^2$	0.83			
$1^3A'$	1.322	1.431	1.490	174.5	104.2	$(10a')^2(2a'')^{\alpha}(11a')^2(12a')^2(3a'')^{\alpha}$	0.95	2.890	3.095	4.2

Table 8
Comparison of the CCCF, CCCCl, and CCCF radicals.

	CCCF			CCCCl			CCCBr		
Renner–Teller type	C			C			C		
State	$1^2\Pi$	X^2A'	$1^2A''$	$1^2\Pi$	X^2A'	$1^2A''$	$1^2\Pi$	X^2A'	$1^2A''$
Parameter									
R_{C1C2} (in Å)	1.364	1.296	1.347	1.339	1.303	1.336	1.335	1.305	1.335
	1.348[a]	1.297[a]			1.308[b]				
R_{C2C3} (in Å)	1.228	1.308	1.225	1.238	1.277	1.239	1.241	1.275	1.241
	1.237[a]	1.301[a]			1.283[b]				
R_{C3X} (in Å)	1.272	1.292	1.268	1.642	1.662	1.636	1.793	1.823	1.793
	1.265[a]	1.284[a]			1.645[b]				
∠C1C2C3 (in °)	180.0	163.3	180.0	180.0	169.5	179.9	180.0	170.4	180.0
	180.0[a]	163.5[a]			169.5[b]				
∠C2C3X (in °)	180.0	134.9	180.0	180.0	142.4	180.0	180.0	142.4	180.0
	180.0[a]	134.8[a]			143.3[b]				
B (in MHz)[c]	4181.0	4500.5	4226.0	2654.0	2825.5	2665.0	1857.0	1971.5	1857.0
	4210.86[a]	4538.51[a]		2674.70[b]	2824.54[b]				
		(4555.8043)[a]			(2848.75)[b]				
Dipole moment (in D)	2.9	2.6	3.1	3.7	3.3	3.7	3.9	3.4	3.9
Barrier to linearity (in cm^{-1})		3106			1519			1276	
		3200[a]			1000[b]				

[a] Taken from Ref. [27].
[b] Taken from Ref. [23].
[c] Value of B_0 for linear molecules and value of $(B + C)/2$ for bent molecules.

We assign the photoelectron data with the vertical IPs for the higher excited states based on the Frank–Condon principle. We hope that these details can give some help to others work since there are no experimental or theoretical details about this. The vertical IPs of the $2^1A'$, $2^3A'$, $1^3A''$, $2^3A''$, $1^1A''$, and $2^1A''$ states are 11.560, 12.419, 12.608, 12.629, 12.943, and 13.126 eV, respectively, which are very close to each other, and these states should correspond to same photoelectron band. Similar results are found in the case of the $3^1A'$, $3^3A'$, $3^3A''$, and $3^1A''$ states. The VIPs of $3^1A'$, $3^3A'$, $3^3A''$, and $3^1A''$ states are 13.482, 13.836, 14.135, and 14.408 eV, respectively, which should be assigned same band. According to the VIPs values, we predict the three bands of PESs around 10.7, 12.5, and 14.0 eV.

3.3. Comparisons among CCCF, CCCCl, and CCCBr

The optimized geometries parameters, dipole moment, and barrier to linearity (ΔE) comparisons among the CCCX radicals(X = F, Cl, and Br) are also performed in Table 8. The fluorine atom is a second row element, the chlorine atom is a third row element, and the bromine is a fourth row element. According to the analysis of linear triatomic Renner–Teller molecules by Lee et al. [43], all of the CCCX radicals are classified as a type C Renner–Teller molecule. The structure parameter of ours are little smaller than the details of Takashi et al. [27].

In the CCCF, CCCCl, and CCCBr, the R_{C1C2}/R_{C2C3} bond distances of 1.296/1.308, 1.303/1.277, and 1.305/1.275 Å are slightly smaller than the C=C double bond in ethylene (1.340 Å). Our calculations exhibit C3 spin densities of 0.7810, 0.6574, and 0.6553 for CCCF, CCCCl, and CCCBr, respectively, which shows that the spin densities of C3 decreases by the electron negativity of X decreasing. The data above indicate the CCCX has the unpaired electron localized on the C3 atom and has allenic bonding, which can be describe as C=C=Ċ—X.

In CCCX, the bent X^2A' state and the nearby linear $1^2A''$ ($1^2\Pi$) state are a Renner–Teller pair derived from the $1^2\Pi$ ground state of the linear molecule. The electron promoted from the HOMO to LUMO pairs up the unpaired electron on the C3 atom, decreasing the R_{C2C3} bond distance and increasing the R_{C1C2} bond distance, generating a C1 centered radical with a linear, acetylenic geometry, which can be described as **.**C—C≡C—F.

The dipole moment of the X^2A' and $1^2A''$ ($1^2\Pi$) states of the CCCX radicals are in order of μ (CCCF) < μ (CCCCl) < μ (CCCBr). The spin–orbital couplings in the CCCX increase as the atomic weight of X increasing [44]. Because the strong spin–orbit couplings can quench the Renner–Teller effect, so our calculated values of the barrier to linear (ΔE) decrease as follows: ΔE (CCCF) > ΔE (CCCCl) > ΔE (CCCBr).

4. Conclusions

Systemic high-level *ab initio* calculations were performed to study and characterized several electronic states of neutral, cation and anion of CCCF radical using aug-cc-pVTZ basis sets and CASSCF/CASPT2 methods.

We predict the geometries of several states of C_3F. The X^2A' state is confirmed as the ground state of C_3F, the calculated rotational constant $\overline{B}$ are in good agreement with experimental and previously theoretical data. At the CASSCF/CASTP2 level, the T_v value of the electron transition from X^2A' state to $1^2A''$ ($1^2\Pi$) is 9880 cm^{-1}, which is very close to theoretical value (10,000 cm^{-1}) [27]. The vertical excitation energies are predicted at 2.893 and 4.180 eV for $X^2A' \rightarrow 3^2A''$ and $\rightarrow 5^2A'$ of CCCF. The structure of ground state X^1A' for $CCCF^+$ is to be linear, while the structure of ground state X^1A' for $CCCF^-$ is strongly bent. For $CCCF^-$, the T_a values of the $1^1A''$ and $2^1A'$ states have been predicted at 1.689 and 2.833 eV. The magnitude of the dipole moment is larger for the anionic states. The first AEA of CCCF is calculated to be 2.550 eV. The AIPs and VIPs at the CASSCF/CASPT2 levels are more than 9 eV. According to the VIPs values, we predicted the three bands of PES around 10.7, 12.5, and 14.0 eV.

In the ground state, the CCCX radicals have an allenic (C—C—Ċ—X) electronic structure with unpair electron on C3 atom, but are more appropriately described as having an acetylenic (**.**C—C≡C—X) structure in the first excited states, with the unpaired electron localized on the C1 atom. The larger Renner–Teller effect for CCX bending compared to CCC bending in all these radicals is a direct result of the larger dipole moment component generated by displacing the X atom from linearity. The Renner–Teller stabilization energies (ΔE) are smaller as atomic weight of X increase.

Acknowledgment

This work was supported by the Natural Science Foundation of China (Grant No. 20973076).

References

[1] M. Guélin, S. Green, P. Thaddeus, Astrophys. J. 224 (1978) L27.
[2] J. Cernicharo, C. Kahane, J. Gómez-Gonzáles, M. Guélin, Astron. Astrophys. 164 (1986) L1.
[3] P. Thaddeus, C.A. Gottlieb, Å. Hjalmarson, L.E.B. Johansson, W.M. Irvine, P. Friberg, R.A. Linke, Astrophys. J. 294 (1985) L49.
[4] P. Friberg, Å. Hjalmarson, W.M. Irvine, M. Guélin, Astrophys. J. 241 (1980) L99.
[5] E.D. Tenenbaum, A.J. Apponi, L.M. Ziurys, M. Agúndez, J. Cerni-charo, J.R. Pardo, M. Guélin, Astrophys. J. 649 (2006) L17.
[6] N. Sakai, M. Ikeda, M. Morita, T. Sakai, S. Takano, Y. Osamura, S. Yamamoto, Astrophys. J. 663 (2007) 1174.
[7] P. Botschwina, J. Mol. Struct.: Theochem. 724 (2005) 95.
[8] H. Wang, J. Szczepanski, P. Brucat, M. Vala, Int. J. Quantum Chem. 102 (2005) 795.
[9] H.Y. Wang, J. Szczepanski, A. Cooke, P. Brucat, M. Vala, Int. J. Quantum Chem. 102 (2005) 806.
[10] A. Zaidi, S. Lahmar, Z. Ben Lakhdar, P. Rosmus, M. Hochlaf, Theor Chem. Acc. 114 (2005) 341.
[11] L. Antonio, C. Alvaro, R.B. Pilar, Carmen 84 (2001) 127.
[12] Y. Endo, S. Saito, E. Hirota, J. Mol. Spectrosc. 94 (1982) 199.
[13] C. Yamada, K. Nagai, E. Hirota, J. Mol. Spectrosc. 85 (1981) 416.
[14] J.B. Burkholder, A. Sinha, P.D. Hammer, C.J. Howard, J. Mol. Spectrosc. 127 (1988) 61.
[15] P. Jin, B.C. Chang, R. Fei, T.J. Sears, J. Mol. Spectrosc. 182 (1997) 189.
[16] P. Venkateswarlu, Phys. Rev. 77 (1950) 79.
[17] R.D. Verma, R.S. Mulliken, J. Mol. Spectrosc. 6 (1961) 419.
[18] R.D. Gordon, G.W. King, Can. J. Phys. 39 (1961) 252.
[19] H. Bredohl, I. Dubois, F. Melen, J. Mol. Spectrosc. 98 (1983) 495.
[20] Y. Sumiyohsi, T. Ueno, Y. Endo, J. Chem. Phys. 119 (2003) 1426.
[21] J. van Wijngaarden, A. Batalov, I. Shnitko, J. Fulara, J.P. Maier, J. Phys. Chem. A 108 (2004) 4219.
[22] J. van Wijngaarden, I. Shnitko, A. Batalov, P. Kolek, J. Fulara, J.P. Maier, J. Phys. Chem. A 109 (2005) 5553.
[23] T. Yoshikawa, Y. Sumiyoshi, Y. Endo, J. Chem. Phys. 130 (2009) 094302.
[24] P. Redondo, J. Redondo, C. Barrientos, A. Largo, Chem. Phys. Lett. 315 (1999) 224.
[25] A. Largo, A. Cimas, P. Redondo, C. Barrientos, Int. J. Quantum Chem. 84 (2001) 127.
[26] L.B. Wang, W.P. Wu, J.L. Zhang, Z.X. Cao, J. Mol. Struct.: Theochem. 773 (2006) 81.
[27] Y. Takashi, S. Yoshihiro, E. Yasuki, J. Chem. Phys. 130 (2009) 164303.
[28] C.Y. Hou, H.X. Zhang, C.C. Sun, J. Phys. Chem. A 110 (2006) 10260.
[29] C.Y. Hou, Q.C. Zheng, Z.X. Zhao, H.X. Zhang, J. Phys. Chem. A 111 (2007) 12037.
[30] Z.Z. Wei, B.T. Li, H.X. Zhang, C.C. Sun, K.L. Han, J. Comput. Chem. 28 (2007) 467.
[31] B.T. Li, Z.Z. Wei, H.X. Zhang, C.C. Sun, J. Phys. Chem. A 110 (2006) 10643.
[32] Z.X. Zhao, H.X. Zhang, C.C. Sun, J. Phys. Chem. A 112 (2008) 12125.
[33] Z.X. Zhao, C.Y. Hou, X. Shu, H.X. Zhang, C.C. Sun, Theor. Chem. Acc. 124 (2009) 85.
[34] Y.J. Liu, Z.X. Zhao, H.X. Zhang, C.C. Sun, Theor. Chem. Acc. 125 (2010) 65.
[35] Y.J. Liu, M.B. Huang, Chem. Phys. Lett. 360 (2002) 400.
[36] M.X. Song, Z.X. Zhao, F.Q. Bai, Y.J. Liu, H.X. Zhang, C.C. Sun, J. Phys. Chem. A 114 (2010) 7173.
[37] B.O. Roos, in: K.P. Lawley (Ed.), Advance in Chemical Physica: Ab Initio Methods in Quantum Chemistry-II, John Wiley & Sons, Chichester, England, 1987, p. 399 (Chapter 69).
[38] K. Andersson, P. Malmqvist, B.O. Roos, A.J. Sadlej, K. Wolinski, J. Phys. Chem. 94 (1990) 5483.
[39] A.R.W. McKellar, P.R. Bunker, T.J. Sears, K.M. Evenson, R.J. Saykally, S.R. Langhoff, J. Chem. Phys. 79 (1983) 5251.
[40] R.A. Kendall, T.H. Dunning Jr, R.J. Harrison, J. Chem. Phys. 96 (1992) 6769.
[41] P.Å. Malmqvist, B.O. Roos, Chem. Phys. Lett. 155 (1989) 189.
[42] K. Andersson et al., LCAS, Version 6.0, University of Lund, Sweden, 2004.
[43] T.J. Lee, D.J. Fox, H.F. Schaefer III, J. Chem. Phys. 81 (1984) 356.
[44] V.K. Igor, A.S. Yuri, J.T. Nicholas, Chem. Rev. 93 (1993) 537.